

Lagrange Gradient Mask for Optical Image Processing

Falih Ahmad^{*,1}, Matthew Gilbert¹, Stephen Myers¹, José Pacheco¹, Ray Castellane² and Ernest Miller²

¹Department of Mathematics, Physics and Engineering, Tarleton State University, Stephenville, TX 76402, USA

²Department of the Army, Engineer Research and Development Center, Waterways Experiment Station, 3909 Halls Ferry Road, Vicksburg, MS 39180, USA

Abstract: Masks are used in optical image processing. They are used to generate gradient maps. These maps are applicable to the enhancement of feature extraction and edge detection. Lagrange mask is presented in this letter and criteria for the characterizations of mask performance are given. Through an illustration the performance of the presented mask is demonstrated where it is compared to that of Gabor mask. Results from the illustration support the applicability and suitability of Lagrange mask for the generation of gradient maps from a noise corrupted optical image.

1. INTRODUCTION

Extracting features from complex optical images is considered a challenging task. Optical image processing techniques are proposed for carrying out such a task where gradient masks are used [1-3]. From the application point of view, as gradient masks are applied to optical images, corresponding gradient maps are generated. For example three image processing steps are applied in [4] to detect the distance between two endocardium from a digitally produced optical image. This is useful for the analysis of heart disease. The steps are: optical image improvement, detecting edges from these images using Sobel gradient mask, and contour line generation. In [5] spatial/temporal gradients of the intensity of an optical image are used for accurate passive ranging. In this case, gradient estimation is performed with a space/time Sobel mask. In [6] a stochastic gradient operator is significantly improved and recommended for the detection of edges in noisy optical images. The improvement is achieved by incorporating three additional features. Namely, robust estimation of the noise variance and the autocorrelation function of the signal, adaptation of a gradient mask, and threshold calculation. Notably, an extensive study of gradient mask design principles is presented in [7]. In particular, the performance of the Gabor mask for edge detection is investigated in [8] using the criteria proposed in [9] and gradient maps are produced in [10] utilizing fine and coarse Gabor masks. Eventually, the produced maps are used for feature extraction through wavelet transform. A presentation of the basic method used to generate the magnitude of the gradient maps of images is given in [11] where it is shown to be an inner product between the image and the mask.

Quality of the gradient maps is an important part of an optical image processing procedure in which edge detection is a subsequent step. The use of edge detection for feature

extraction is one of many applications of vision systems. In many applications detection of edges is performed in optical images corrupted by noise. In [12] an adaptive method for noise reduction and edge detection is developed. This method is based on the minimum mean square error estimate. One- and two-dimensional finite impulse response filters are used in [13] for dealing with the detection of edges of noisy images. In another case, prior to noise reduction, logarithmic transformation is applied to a noisy image to convert the multiplicative noise to an additive noise [14]. Consequently, it is noted here that it would be appreciated if the gradient map generating mask was able to increase the signal to noise ratio prior to subsequent steps taken toward edge detection or feature extraction from a noise corrupted optical image.

In this letter Lagrange mask is presented. Selected discrete versions of the criteria developed by Canny which are given in [15] are used for mask performance characterization. The method of using a mask and producing a gradient map from an image given in [11] and the edge detector developed in [9] are applied. For comparison purposes, Gabor mask is used. Through a performance illustration the applicability and suitability of Lagrange mask to optical image processing is demonstrated.

The letter is organized as follows. In section 2 the formulations of Lagrange and Gabor masks are given. Criteria used for mask characterization are presented in section 3. In section 4 a performance illustration is given in which mask performance results are demonstrated.

2. LAGRANGE AND GABOR MASKS

2.1. Formulation of Lagrange Mask

Lagrange polynomials of order k are given as [16]

$$\psi_k(\tau) = \frac{(\tau^2 - 1)\dot{L}_M(\tau)}{M(M+1)(\tau - \tau_k)L_M(\tau_k)}, \quad k = 0, 1, \dots, M \quad (1)$$

Equation (1) exhibit the Dirac delta property

*Address correspondence to this author at the Department of Mathematics, Physics and Engineering, Tarleton State University, Stephenville, TX 76402, USA; E-mail: AHMAD@tarleton.edu

$$\psi_k(\tau_j) = \delta_{kj} = \begin{cases} 0, & \text{if } k \neq j \\ 1, & \text{if } k = j \end{cases}$$

and $L_M(\tau)$ is Legendre polynomial of order M , $-1 \leq \tau \leq 1$, $\tau_0 = -1$, $\tau_M = 1$ and τ_l , $1 \leq l \leq M-1$, are the zeros of the first derivative of Legendre polynomial, $L'_M(\tau)$. They are the abscissas for Lobatto integration [17]. The result of differentiating equation (1) with respect to τ , ψ_{kl} , is [16]

$$\psi_{kl} = \psi_l(\tau_k) = \begin{cases} \frac{L_M(\tau_k)}{L_M(\tau_l)(\tau_k - \tau_l)} & \text{if } k \neq l \\ \frac{M(M+1)}{4} & \text{if } k = l = 0 \\ -\frac{M(M+1)}{4} & \text{if } k = l = M \\ 0 & \text{Otherwise} \end{cases} \quad (2)$$

Equation (2) is used to generate a matrix of size $(M-1) \times (M-1)$. As seen from this equation, the diagonal elements of this matrix are zero except the end elements. Furthermore, the upper and lower triangles of this matrix form an odd symmetry configuration. This property allows for the production of masks of odd symmetry of dimension $N \times N$, $N < M-1$. This is a property similar to that of Gabor mask which presented in section 2.2. In contrast to Gabor mask, it should be noted, however, that the nodes at which the elements of this mask are generated are non-uniformly distributed within the interval $[-1, 1]$. The characteristics of Legendre and Lagrange polynomials were the main reason for proposing Lagrange mask here.

2.2. Formulation of Gabor Mask

A general spatial equation used to formulate Gabor masks considered here is [8]

$$G(x, y) = e^{-0.5 \left(\frac{x^2 + y^2}{\sigma^2} \right)} \sin[\omega(x \cos \theta + y \sin \theta)] \quad (3)$$

Specifically, Gabor masks can be produced with $\sigma = 1$, $\theta = 0$, $\omega = 1$, and x values from the interval $[-\pi, \pi]$, [10]. The desired size of the mask dictates the number of points at which Equation (3) is evaluated. These points are uniformly distributed within the interval from which they are taken.

3. CHARACTERIZATION CRITERIA

Four criteria are used for the purpose of mask performance characterization. The production of an edge map from a gradient map that corresponds to the mask is one criterion. The edge detector given in [9] along with the method of producing gradient maps given in [11] are used in this criterion. The additional three criteria are discrete good detection,

exact localization probability, and noise maximum probability [15]. Information regarding the four criteria is given below:

3.1. Image Gradient Map

Let S and I be the considered mask and image, respectively. The estimated discrete gradient map, GM , that corresponds to I is produced using [11]

$$GM = \sqrt{\text{trace}^2(S^T I) + \text{trace}^2(SI)} \quad (4)$$

It is clear from Equation (4) that the characteristics of the gradient map of a given image are functions of the characteristics of the mask used. This process is followed by edge detection using the edge detector from [9].

3.2. Discrete Good Detection

The discrete good detection criterion is a function of the mask's impulse response. It is given as [15]

$$CD = \frac{\sum_{k=-\infty}^0 h(k)}{\sqrt{\sum_{k=-\infty}^{+\infty} h^2(k)}} \quad (5)$$

The k^{th} value of the mask's impulse response is represented by $h(k)$ in Equation (5). This criterion is a measure of the ability of the mask to maximize the signal to noise ratio [15].

3.3. Exact Localization Probability

A Gaussian random sequence and values of the impulse response of the mask are used to represent two correlated random variables with zero mean and of same variance in [15]. As a function of the impulse response, the corresponding discrete correlation coefficient, ρ , is given as [15]

$$\rho = \frac{\sum_{k=-\infty}^{+\infty} [h(k) - h(k-1)] \cdot [h(k) - h(k+1)]}{\sum_{k=-\infty}^{+\infty} [h(k) - h(k-1)]^2} \quad (6)$$

It is shown in [15] as the value of ρ increases the probability that the mask accurately localizes a step in the presence of white Gaussian noise increases. The dependence of this probability on ρ supports its discrete nature.

3.4. Noise Maximum Probability

In the case where only noise is present, the probability to obtain a maximum induced by noise that can be located by the mask is given as [15]

$$P_n = \frac{\cos^{-1}(\rho)}{2\pi} \quad (7)$$

Values of ρ close to -1 are desired, where at this value Equation (7) is seen to be zero. Here also the dependence of this probability on ρ supports its discrete nature.

4. PERFORMANCE ILLUSTRATION

In this illustration a red, green, and blue (*RGB*) optical image corrupted with an additive Gaussian noise of zero mean and a variance of 0.15 was used as a test image. The signal to noise ratios, in *dB*, of the *R*, *G*, and *B* components of the noise corrupted image were 1.2231, 1.1704, and 1.1231, respectively. The size of the Lagrange, L_m , and Gabor, G_m , masks used to generate their corresponding gradient maps from the test image was 7×7 , each. The masks were generated using Equation (2) with $M = 10$ and Equation (3). They are given in Equations (8) and (9) below.

$$L_m =$$

$$\begin{bmatrix} -1.0000 & -1.5701 & -1.8634 & 0 & 1.8634 & 1.5701 & 1.0000 \\ -0.7336 & -1.1114 & -3.1840 & 0 & 3.1840 & 1.1114 & 0.7336 \\ -0.7918 & -0.9613 & -2.7539 & 0 & 2.7539 & 0.9613 & 0.7918 \\ -0.7383 & -1.3770 & -1.3770 & 0 & 1.3770 & 1.3770 & 0.7383 \\ -0.7918 & -0.9613 & -2.7539 & 0 & 2.7539 & 0.9613 & 0.7918 \\ -0.7336 & -1.1114 & -3.1840 & 0 & 3.1840 & 1.1114 & 0.7336 \\ -1.0000 & -1.5701 & -1.8634 & 0 & 1.8634 & 1.5701 & 1.0000 \end{bmatrix} \quad (8)$$

$$G_m = \begin{bmatrix} 0 & -0.0005 & -0.0021 & 0 & 0.0021 & 0.0005 & 0 \\ 0 & -0.0061 & -0.0254 & 0 & 0.0254 & 0.0061 & 0 \\ 0 & -0.0275 & -0.1140 & 0 & 0.1140 & 0.0275 & 0 \\ 0 & -0.0453 & -0.1880 & 0 & 0.1880 & 0.0453 & 0 \\ 0 & -0.0275 & -0.1140 & 0 & 0.1140 & 0.0275 & 0 \\ 0 & -0.0061 & -0.0254 & 0 & 0.0254 & 0.0061 & 0 \\ 0 & -0.0005 & -0.0021 & 0 & 0.0021 & 0.0005 & 0 \end{bmatrix} \quad (9)$$

For the purpose of mask performance characterization and map production, the following steps were performed:

1. The criteria presented in subsections 3.2 through 3.4 were used to characterize the masks given in Equations (8) and (9); the results are given in Table 1. Notice the closeness of the numbers in each column.

Table 1. Discrete Criteria Results

Mask Type	CD in dB	ρ	P_n
Lagrange	1.1027	-0.1771	0.2203
Gabor	0.8253	0.04748	0.2576

2. In this step criterion 3.1 was utilized. Applying the method given in [11], two (*RGB*) gradient maps from the test image that correspond to G_m and L_m were produced. The noise corrupted test image and its gradient maps are shown in Fig. (1a) below.

3. Edge detection was performed in this step. The colors in each gradient map were treated individually. As a result three edge maps were generated using the edge detector given in [9] with optimum threshold. The edge maps due to L_m are shown in Fig. (1b) and those due to G_m are shown in Fig. (1c). It is noted that deductions can be constructed from comparison of maps by way of visual inspection [18]. A visual inspection of these figures reveals the ability of L_m to locate and accentuate edges from the noise corrupted test image.

Next, *dB* values of signal to noise ratios of the *R*, *G*, and *B* components were decreased to 1.101, 1.0534, and 1.0108, respectively. The procedure presented here was repeated. Again, the produced maps due to Lagrange mask were superior to those due to Gabor mask. On the other hand, further simulation experiments indicated that increasing the kernel size produced finer maps and decreasing its size produced coarse maps. However, this practice did not affect the perspective of the performance of the considered masks.

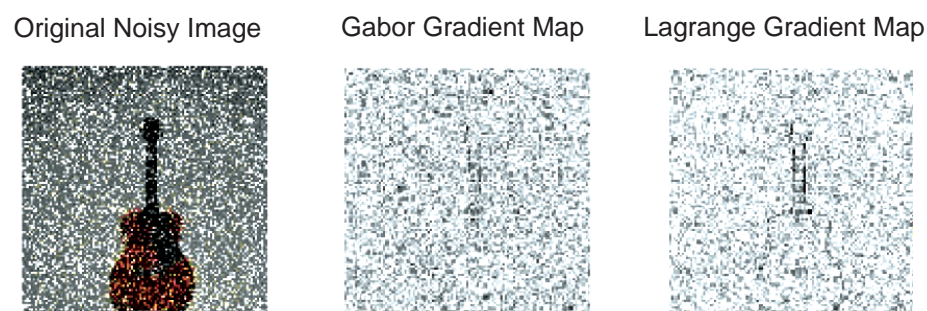


Fig. (1a). Noise corrupted test image and gradient maps.

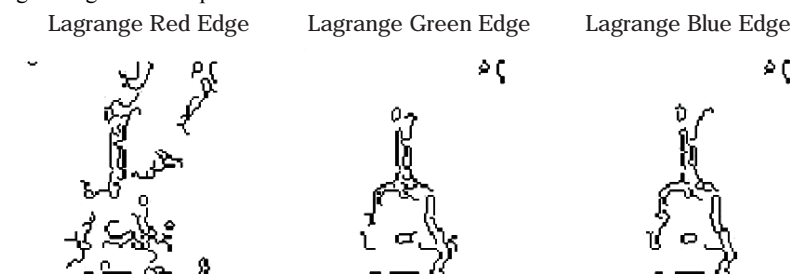


Fig. (1b). Edge maps from (*RGB*) gradient maps due to lagrange mask.



Fig. (1c). Edge maps from (RGB) gradient maps due to gabor mask.

5. CONCLUSIONS

Gradient maps of optical images are an important part of their processing. They are beneficial for edge detection and feature extraction. Gradient maps from such images are generated using masks. Lagrange and Gabor masks are used in this letter for gradient maps generation. These masks share the property of odd symmetry. However, the locations of the elements of Gabor mask are uniformly distributed and those of Lagrange mask are non-uniformly distributed. A noise corrupted optical image was used as a test image in this letter and four criteria were used to characterize the performance of the used masks. Numerical and visual results support the applicability and suitability of Lagrange mask for optical image processing in the presence of additive Gaussian noise. Contributions to the well behavior of Lagrange mask in the presence of noise are due to two major sources. The first is the Dirac delta property that is inherited in its structure, and the second is the non-uniform distribution of the points at which it is evaluated. These properties make Lagrange mask unique with a novel ability of preserving pixel information in the presence of noise. In this way, as it is applied for extraction of features from optical images a great potential benefit is provided.

ACKNOWLEDGEMENTS

This work was supported by the Department of Defense, Engineering Research and Development Center, ERDC, Vicksburg, Mississippi under contract W912HZ-06-P-0007. The authors would like to extend their sincere thanks to Mrs. Pamela Kinnebrew, Chief, Survivability Engineering Branch, ERDC. They also would like to thank Mr. Bartley P. Durst from the Survivability Engineering Branch for valuable subject related conversations. Permission was granted by the Chief of Engineers from ERDC to publish this information.

REFERENCES

- [1] Casasent D, Chen J. Nonlinear Local Image Preprocessing Using Coherent Optical Technique. *Appl Opt* 1983; 22: 808-14.
- [2] Eichmann G, Kostrzewski A, Ha B, Li Y. Parallel Optical Pyramidal Image Processing. *Optics Lett* 1988; 13: 431-3.
- [3] Cherri A, Karim M. Optical Image Processing Using Symbolic Substitution: Median Filtering and Edge Detection: Proceedings of the IEEE 1989 National Aerospace and Electronics Conference; May 1989; IEEE, Dayton, OH, USA; 1989.
- [4] Boonchieng E, Boonchieng W, Kanjanavanit R. Edge-Detection and Segmentation Method for Two-Dimensional Echocardiograms. *Comput Cardiol* 2004; 31: 541-4.
- [5] Lopez J, Markel M, Siddiqi N, Gebert G. Performance of Passive Ranging from Image Flow: Proceedings of the International Conference on Image Processing (ICIP 2003); September 2003; IEEE, Barcelona, Catalonia, Spain; 2003.
- [6] Das M, Anand J. Robust Edge Detection in Noisy Images Using an Adaptive Stochastic Gradient Technique: Proceedings of the International Conference on Image Processing (ICIP 1995); October 1995; IEEE, Washington, DC, USA; 1995.
- [7] Climent J, Grau A, Anand J, Martinez A. A High Precision Operator to Determine Edge Orientation: Conference Publication No. 455 of UKACC International Conference on Control '98; September 1998; IEE, Swansea, UK; 1998.
- [8] Namuduri K, Mehrotra R, Ranganathan N. Edge Detection Models Based on Gabor Filters: Proceedings of the 11th IAPR International Conference on Pattern Recognition, Conference C: Image, Speech and Signal Analysis; August 1992; IEEE, The Hague, Netherland; 1992.
- [9] Canny J. A Computational Approach to Edge Detection. *IEEE Trans Pattern Ana Mach Intelligence* 1986; 8: 679-98.
- [10] Udomhunsakul S, Wongsita P. Feature Extraction in Medical MRI Images: Proceedings of the Conference on Cybernetics and Intelligent Systems; December 2004; IEEE, Singapore; 2004.
- [11] Meer P, Georgescu B. Edge Detection with Embedded Confidence. *IEEE Trans Pattern Ana Mach Int* 2001; 23: 1351-65.
- [12] Sun X, Venetsanopoulos A. Adaptive Schemes for Noise Filtering and Edge Detection by Use of Local Statistics. *IEEE Trans Circ Sys* 1988; 35: 57-69.
- [13] Leung C, Lu W. Detection of Edges of Noisy Images by 1-D and 2-D Linear FIR Digital Filter: Proceedings of the Pacific Rim Conference on Communications, Computers and Signal Processing; May 1993; IEEE, Victoria, BC, Canada; 1993.
- [14] Udomhunsakul S. Edge Detection in Ultrasonic Image Using Gabor Filters: Proceedings of the TENCON IEEE Region Conference; November 2004; IEEE, Chiang Mai, Thailand; 2004.
- [15] Demigny D, Kamlé T. A Discrete Expression of Canny's Criteria for Step Edge Detector Performances Evaluation. *IEEE Trans Pattern Ana Mach Int* 1997; 19: 1199-211.
- [16] Canuto C, Hussaini M, Quarteroni A, Zang T. Spectral Methods in Fluid Dynamics. Springer-Verlag: Berlin; 1987.
- [17] Abramowitz M, Stegun I. Handbook of Mathematical Functions. Dover: New York; 1972.
- [18] Pratt W. Spatial Transform Coding of Color Images. *IEEE Trans Comm Tech* 1971; 19: 980-92.